Article

Not peer-reviewed version

Atrial TRPM2 Channel-Mediated Ca^{2+} Influx Regulates ANP Secretion and Protects Against ISO-Induced Cardiac Hypertrophy and Fibrosis

Tomohiro Numata *, Hideaki Tagashira, Kaori Sato-Numata, Meredith C. Hermosura, Fumiha Abe, Ayako Sakai, Shinichiro Yamamoto, Hiroyuki Watanabe

Posted Date: 17 November 2025

doi: 10.20944/preprints202511.1147.v1

Keywords: TRPM2; atrial natriuretic peptide (ANP); calcium signaling; cardiac hypertrophy; fibrosis; beta-adrenergic stress; cardiac hormones

 doi:10.20944/preprints202511.1147.v1

Article

Atrial TRPM2 Channel-Mediated Ca^{2+} Influx Regulates ANP Secretion and Protects Against ISO-Induced Cardiac Hypertrophy and Fibrosis

Tomohiro Numata [1,*], Hideaki Tagashira [1], Kaori Sato-Numata [1], Meredith C. Hermosura [2], Fumiha Abe [1], Ayako Sakai [1], Shinichiro Yamamoto [3] and Hiroyuki Watanabe [4]

[1] Department of Integrative Physiology, Graduate School of Medicine, Akita University, Akita, Japan
[2] John A. Burns School of Medicine, Honolulu, HI, USA
[3] Faculty of Pharmaceutical Sciences, Teikyo Heisei University, Tokyo, 164-8530, Japan
[4] Department of Cardiovascular Medicine, Akita University Graduate School of Medicine, Akita, Japan
* Correspondence: numata@med.akita-u.ac.jp; Tel.: +81-18-884-6272

Highlights

What are the main findings?

1. TRPM2 is functionally enriched in atrial cardiomyocytes and drives stress-evoked Ca^{2+} influx that triggers ANP secretion.
2. TRPM2 deficiency exacerbates ISO-induced hypertrophy, fibrosis, and systolic dysfunction, with blunted *Nppa*/ANP induction; exogenous ANP rescues these phenotypes.

What are the implications of the main findings?

1. The study defines a TRPM2–Ca^{2+}–ANP axis linking oxidative/β-adrenergic stress to atrial endocrine output.
2. Therapeutic augmentation of the ANP axis (e.g., ANP administration, neprilysin inhibition) or targeting TRPM2 may mitigate pathological cardiac remodeling in hypertension and heart failure.

Abstract

Transient receptor potential melastatin 2 (TRPM2) channel is a Ca^{2+}-permeable, redox-activated cardiac ion channel protective in ischemia–reperfusion, but whether it regulates atrial endocrine output under stress is unclear. We compared how wild-type (WT) and TRPM2 knockout ($TRPM2^{-/-}$) mice respond to β-adrenergic stress induced by isoproterenol (ISO) using echocardiography, histology, RT-PCR, electrophysiology, Ca^{2+} imaging, ELISA, and atrial RNA-seq. We detected abundant Trpm2 transcripts in the atria of WT mice, and measured ADP-ribose (ADPr)–evoked currents as well as hydrogen peroxide (H_2O_2)–induced Ca^{2+} influx characteristic for TRPM2 of WT atrial myocytes; these were absent in $TRPM2^{-/-}$ cells. Under the ISO-induced hypertrophic model, $TRPM2^{-/-}$ mice developed greater cardiac hypertrophy, fibrosis, and systolic dysfunction compared with WT mice. Atrial bulk RNA-seq showed significant induction of *Nppa* (ANP precursor gene) in WT + ISO, accompanied by higher circulating ANP; $TRPM2^{-/-}$ + ISO showed blunted *Nppa* and ANP responses. ISO-treated $TRPM2^{-/-}$ mice exhibited more blunt responses, in both *Nppa* transcripts and circulating ANP levels. Exogenous ANP attenuated ISO-induced dysfunction, hypertrophy, and fibrosis in $TRPM2^{-/-}$ mice, suggesting that TRPM2 is needed for the cardioprotective endocrine response via ANP to control stress-induced β-adrenergic remodeling.

Keywords: TRPM2; atrial natriuretic peptide (ANP); calcium signaling; cardiac hypertrophy; fibrosis; beta-adrenergic stress; cardiac hormones

1. Introduction

 doi:10.20944/preprints202511.1147.v1

Cardiac hypertrophy and fibrosis are hallmark features of pathological remodeling in response to chronic β-adrenergic stimulation, as seen in conditions such as hypertension and heart failure [1–5]. In these settings, reactive oxygen species (ROS) act as active amplifiers of maladaptive signaling, arising from mitochondrial and enzymatic sources, and promote pro-hypertrophic and pro-fibrotic pathways [6–10]. Atrial natriuretic peptide (ANP), secreted primarily by atrial cardiomyocytes, plays a pivotal endocrine role in attenuating cardiac remodeling by promoting natriuresis, vasodilation, and antifibrotic signaling [11–13]. Accordingly, regulated ANP secretion is a critical adaptive mechanism; however, the upstream molecular triggers that govern ANP release under stress conditions remain incompletely understood.

The transient receptor potential melastatin 2 (TRPM2) channel is a Ca^{2+}-permeable, non-selective cation channel activated by oxidative stress, ADPr, and hypertonicity [14–17]. TRPM2 is expressed in a wide variety of cells and tissues, including the cardiovascular system, where it has been implicated in redox/inflammatory signaling, cardioprotection against ischemia–reperfusion (I/R) injury [18], and in vascular/endothelial biology [19,20]. Mechanistically, oxidative DNA damage can activate PARP/PARG, elevating free ADPr that binds to the TRPM2 NUDT9-H domain to gate the channel and facilitate Ca^{2+} influx [15,21,22]. Studies using ventricular myocytes have provided evidence ascribing the protective effects of TRPM2 to Ca^{2+} entering the channel [23] and causing the phosphorylation of Pyk2, which in turn translocates to the mitochondria, thereby improving mitochondrial bioenergetics and maintaining cardiac health [24,25].

In preliminary studies, we found robust expression of TRPM2 transcripts in atrial cardiomyocytes. Given that the cardiac hormone ANP is primarily produced by atrial cardiomyocytes, we wondered if Ca^{2+} entering through TRPM2 channels influences the production and/or secretion of ANP, thereby providing an upstream Ca^{2+} signal that triggers ANP release in response to β-adrenergic stress. We hypothesize that TRPM2-mediated Ca^{2+} entry in atrial cardiomyocytes contributes to stress-evoked ANP release. We tested this hypothesis by investigating the role of TRPM2 in atrial endocrine signaling and its relationship to cardiac remodeling using WT and TRPM2 knockout ($TRPM2^{-/-}$) mice subjected to isoproterenol (ISO)–induced β-adrenergic stress. This framework guided our experimental design across molecular, cellular, and in vivo analyses.

2. Materials and Methods

2.1. Animals and In Vivo Treatment Protocol

Male wild-type (WT) and TRPM2 knockout ($TRPM2^{-/-}$) mice (provided by Professor Mori, Kyoto University, on a C57BL/6J background (8–12 weeks old), born from the same litters and, were housed under controlled environmental conditions (25 ± 1 °C; 12-h light/dark cycle) with ad libitum access to food and water. To induce pathological cardiac stress, mice received once-daily intraperitoneal injections of isoproterenol (ISO; 30 mg/kg/day) for 7 or 21 consecutive days [26]; age-matched controls were administered volume-matched vehicle. For ANP supplementation, a subset of mice received atrial natriuretic peptide (ANP; 400 μg/kg, s.c.) twice daily for 7 days, administered subcutaneously on the same daily schedule during the ISO protocol; corresponding controls received vehicle. All experimental procedures complied with institutional guidelines and were approved by the Animal Ethics Committee of Akita University (approval nos. a-1-0412 and b-1-0408). Mice were randomly assigned to treatment groups, and outcome assessments were performed by investigators blinded to genotype and treatment.

2.2. Echocardiography

Cardiac function was evaluated by transthoracic echocardiography using the Vevo 770 system (FUJIFILM VisualSonics Inc., Toronto, Canada) under ketamine (50 mg/kg) and xylazine (5 mg/kg) anesthesia. Fractional shortening (FS%), ejection fraction (EF%), left ventricular end-systolic diameter (LVESD), and end-diastolic diameter (LVEDD) were calculated from M-mode tracings.

 doi:10.20944/preprints202511.1147.v1

2.3. Histology and Morphometry

At the endpoint, mice were euthanized by cervical dislocation, and hearts were excised for histological analysis. Heart weight-to-body weight (HW/BW) ratios were determined. Paraffin-embedded sections were stained with hematoxylin–eosin (HE) and Masson's trichrome (MT) to evaluate myocardial hypertrophy and fibrosis. Images were acquired using a BZ-X800 inverted microscope (KEYENCE, Tokyo, Japan). Fibrosis quantification. Masson's trichrome (MT) images were analyzed in Adobe Photoshop (Adobe Systems, San Jose, CA, USA) using a pre-specified, uniform workflow applied to all samples. First, the background signal was minimized by applying the Image Subtract function using a blank-area region of interest sampled on each slide. Next, collagen-positive regions were segmented using the Color Range selection of the MT blue component, with a fixed tolerance determined a priori and held constant across all images. Total tissue area (myocardium only) was obtained by excluding background and non-tissue spaces (e.g., cavities) using thresholding with minor manual cleanup under the same settings. The fibrosis fraction was calculated as the number of blue-positive pixels divided by the total number of tissue pixels, expressed as a percentage.

2.4. Isolation of Atrial and Ventricular Cardiomyocytes

Single cardiomyocytes were isolated by retrograde aortic perfusion (Langendorff method) using Ca^{2+}-free Tyrode's solution, followed by enzymatic digestion with collagenase type II (Worthington, Lakewood, NJ, USA). After digestion, the atria and ventricles were dissected, gently triturated in enzyme-containing solution, and the cell suspensions were filtered and allowed to settle by gravity. Cells were then transferred to the recording buffer. Only quiescent, rod-shaped myocytes with apparent striations were selected. Electrophysiological recordings and Ca^{2+} imaging were performed within 8 h of isolation.

2.5. Whole-Cell Patch-Clamp Electrophysiology

Whole-cell recordings were obtained from isolated atrial myocytes of WT and $TRPM2^{-/-}$ mice at room temperature (22–27 °C). Patch electrodes were pulled from borosilicate glass capillaries using a P-97 puller (Sutter Instrument, Novato, CA, USA) and had tip resistances of 2–5 MΩ (typically 3–5 MΩ). Currents were recorded in the whole-cell configuration using either an EPC-9 amplifier (HEKA Elektronik, Lambrecht, Germany) or an Axopatch 200B amplifier (Axon Instruments/Molecular Devices, Union City, CA, USA). Signals were low-pass filtered at 5 kHz (four-pole Bessel), digitized at 10 or 20 kHz, and acquired/controlled with PULSE v8.8 (HEKA) or pCLAMP v10.0.2 (Molecular Devices). Series resistance was compensated for 70–80% to minimize voltage errors. Only quiescent, rod-shaped cells with apparent striations were analyzed, and current amplitudes were normalized to membrane capacitance (pA/pF).

External (bath) solution (pH 7.2 with NaOH; 320 mOsm): NaCl 145 mM, $MgCl_2 \cdot 6H_2O$ 1.2 mM, $CaCl_2$ 0.2 mM, HEPES 11.5 mM, D-glucose 10 mM. Internal (pipette) solution (pH 7.2 with CsOH; 300 mOsm adjusted with D-mannitol): Cs-hydroxide 105 mM, aspartate 105 mM, CsCl 40 mM, $MgCl_2$ 2 mM, $CaCl_2$ 2.789 mM, K_4-BAPTA 5 mM, Na_2-ATP 2 mM, HEPES 5 mM; ADPr 0.5 mM was included where indicated.

Cells were held at 0 mV and subjected to a ramp protocol consisting of brief square steps to +100 mV (10 ms) and −100 mV (10 ms), followed by a linear ramp from +100 to −100 mV over 100 ms, repeated every 10 s. TRPM2 activity was assessed by comparing I–V relationships recorded with versus without 0.5 mM ADPr in the pipette in WT and $TRPM2^{-/-}$ atrial myocytes.

2.8. Calcium Imaging

Intracellular Ca^{2+} was monitored in freshly isolated atrial myocytes using the ratiometric indicator fura-2 AM (Dojindo Laboratories, Kumamoto, Japan). Cells were incubated with fura-2 AM (5 μM) for 30 min at 37 °C, rinsed for 15 min at room temperature.

 doi:10.20944/preprints202511.1147.v1

Recordings were obtained on an inverted epifluorescence microscope (IX81, Olympus Corp., Tokyo, Japan) equipped with a xenon arc lamp and monochromator (Polychrome IV, TILL Photonics GmbH, Gräfelfing, Germany) and a cooled CCD camera (ORCA series, Hamamatsu Photonics, Shizuoka, Japan). Fura-2 was excited alternately at 340 and 380 nm, and emission was collected through a 510-nm long-pass filter. Image acquisition and ratio calculations (F340/F380) were performed with MetaFluor software (Molecular Devices, San Jose, CA, USA) with fixed exposure across conditions.

All measurements were carried out in Tyrode's solution containing (in mM) NaCl 145, $MgCl_2 \cdot 6H_2O$ 1.2, $CaCl_2$ 0.2, HEPES 11.5, D-glucose 10; pH 7.2 with NaOH, 320 mOsm. After establishing a stable baseline (≥60 s), cells were exposed to H_2O_2 (oxidative stimulus; concentration indicated in figure legends) according to the experimental protocol. Changes in Ca^{2+} were quantified as ΔRatio = peak F340/F380 − baseline F340/F380. Only quiescent, rod-shaped cells with stable baselines were included.

2.9. Primary Culture of Neonatal Mouse Ventricular Myocytes (NMVMs) and Hypertrophy Assay

Neonatal ventricular myocytes were isolated from 1–3-day-old C57BL/6J WT and TRPM2$^{-/-}$ pups using the Pierce Cardiomyocyte Isolation Kit (Thermo Fisher Scientific, Waltham, MA, USA). Cells were cultured in DMEM supplemented with 10% fetal bovine serum, followed by serum-free conditions before stimulation. After 48 h, hypertrophy was induced with isoproterenol (ISO, 10 μM, 24–72h) in the absence or presence of recombinant mouse ANP (0.1 μM; Peptide Institute, Osaka, Japan).

For morphometry, cells were fixed in 4% paraformaldehyde (FUJIFILM Wako Pure Chemical, Osaka, Japan) for 5 min, and the fixed cells were incubated with rhodamine-phalloidin reagent (Abcam, Cambridge, UK) in PBS containing 1% BSA (FUJIFILM Wako) for 1 hour at room temperature. Fluorescence images were acquired using a BZ-X800 microscope (KEYENCE, Tokyo, Japan) with identical exposure and acquisition parameters across conditions.

Cell cross-sectional area (CSA) was quantified from phalloidin images using ImageJ (NIH). For each condition, >100 cells were analyzed from ≥3 independent isolations (biological replicates); the analyst was blinded to genotype and treatment.

2.10. RNA-seq

Total RNA was extracted from mouse atria and ventricles. For each genotype/treatment condition (WT, TRPM2$^{-/-}$, WT+ISO, TRPM2$^{-/-}$+ISO), atria from three mice were pooled at equal tissue mass to generate one composite RNA sample, yielding four composite libraries (one per condition). Library construction and sequencing were performed by Macrogen Japan Corp. (Kyoto, Japan). Stranded poly(A)+ libraries were prepared and sequenced on an Illumina NovaSeq X (Illumina, San Diego, CA, USA), generating paired-end 101-bp FASTQ reads. Pre-processing removed rRNA-derived reads using SortMeRNA v4.3.7 with rRNA references extracted from GCF_000001405.26_GRCh38_rna.fna, followed by adapter and low-quality trimming with Cutadapt v4.9 (Phred cutoff Q20; minimum read length 25 nt). Read quality before and after trimming was assessed with FastQC and summarized with MultiQC. Filtered reads were aligned to the Mus musculus reference genome GRCm38.p6 (RefSeq GCF_000001635.26; genomic FASTA GCF_000001635.26. Functional enrichment used clusterProfiler v4.16.0 with org.Mm.eg.db (v3.21.0). For Gene Ontology (GO; BP/CC/MF) over-representation analysis (ORA), the gene set comprised DE genes with $|\log2FC| \geq 0.26$ (≈20% change) and FDR < 0.05. Gene Set Enrichment Analysis (GSEA) was performed in clusterProfiler on a pre-ranked vector (e.g., signed statistic based on log2FC), with 10,000 permutations, minGSSize = 10, maxGSSize = 500, and significance defined as FDR q < 0.25 (GSEA convention). Pathway analysis used KEGG (Kyoto Encyclopedia of Genes and Genomes) gene sets within the same framework and genome build. GO/GSEA/KEGG outputs are reported as normalized enrichment score (NES), FDR q-value, and leading-edge genes, with full ranked lists and enrichment tables provided in Supplementary Data.

 doi:10.20944/preprints202511.1147.v1

2.11. RT-PCR and Quantitative PCR

Total RNA was prepared as described in Section 2.10. cDNA was synthesized using ReverTra Ace® qPCR RT Master Mix (TOYOBO Co., Ltd., Osaka, Japan) with random hexamers/oligo(dT) primers.

Conventional RT-PCR. Targets (*Trpm2*, *Nppa* (ANP), *Npr1* (NPR-A)) and housekeeping genes (*Gapdh*, *Actb* (β-actin)) were amplified using TOYOBO PCR reagents (e.g., KOD One™ PCR Master Mix, TOYOBO). Products were separated on agarose gels and visualized using SYBR™ Safe (Thermo Fisher Scientific) to confirm single bands at the expected sizes (representative gels shown in Figure 1).

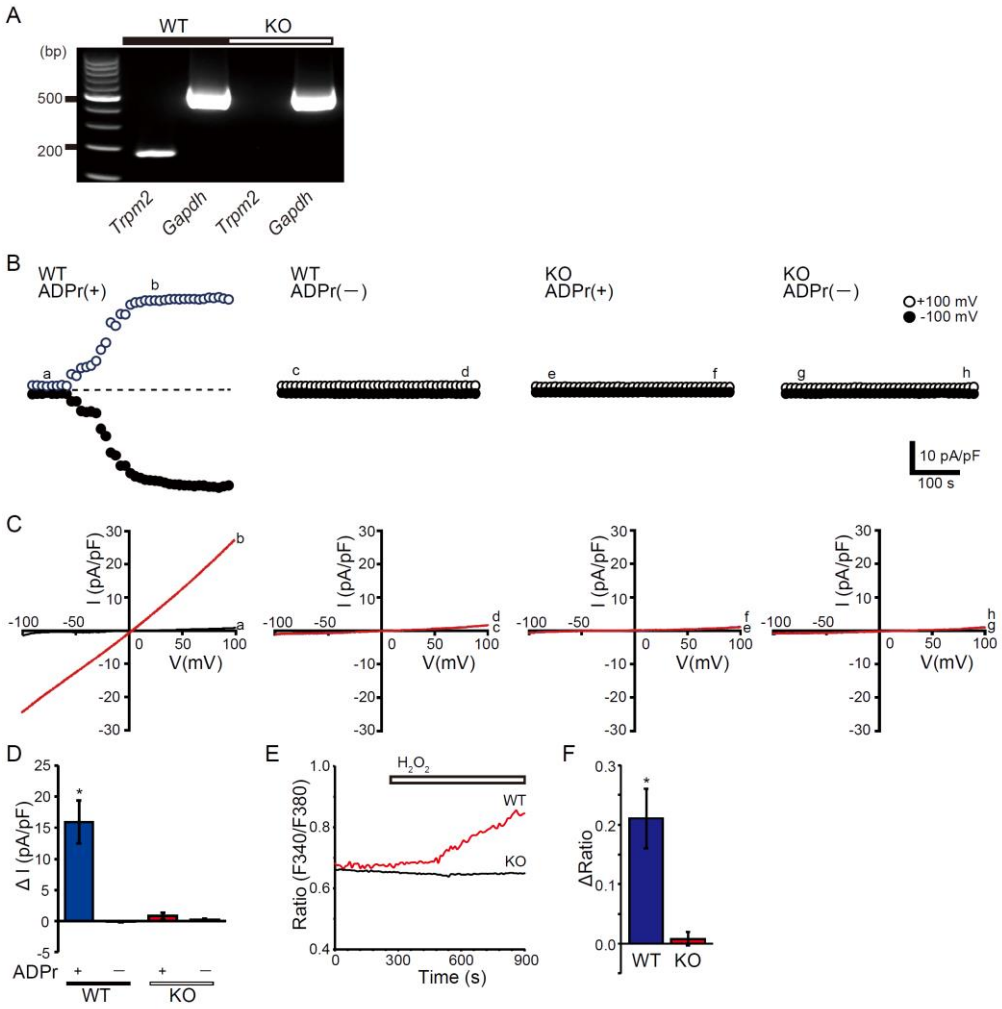

Figure 1. Atrial TRPM2 expression and TRPM2-dependent Ca^{2+} signals. (A) RT-PCR of *Trpm2* and *Gapdh* from atria in WT and TRPM2$^{-/-}$ (KO) mice; representative gel images are shown. *Gapdh* is the loading control. (B) Whole-cell patch clamp from isolated atrial myocytes: time courses of currents at +100 mV (open symbols) and −100 mV (filled symbols) recorded with 0.5 mM ADP-ribose in the pipette (ADPr (+)) or without ADPr (ADPr (−)). The horizontal dotted line denotes the zero-current baseline. (C) Corresponding I–V relationships (ramps from +100 to −100 mV) at the indicated time points (a–h in panel B). (D) Summary of ADPr-activated current density (ΔI at +100 mV, pA/pF). Statistics evaluate within-genotype ADPr (+) vs ADPr (−). $^{*}p < 0.05$ vs ADPr (−). (E) Fura-2 ratiometric Ca^{2+} imaging in atrial myocytes during extracellular H_2O_2 (200 μM; bar) in Tyrode's solution. (F) Quantified peak ΔRatio from (E). $^{*}p < 0.05$ vs KO.

qPCR. Quantitative PCR was performed with THUNDERBIRD® SYBR® qPCR Mix (TOYOBO) on a LightCycler® 480 system (Roche Diagnostics, Basel, Switzerland). Targets were *Nppa*, and *Npr1*. *Gapdh* served as the reference gene (with β-actin used for confirmation, where indicated). Reactions

 doi:10.20944/preprints202511.1147.v1

were run in technical triplicates; specificity was verified by melting-curve analysis. Relative expression was calculated using the $2^{-}\Delta\Delta Ct$ method. Primer sequences and expected amplicon sizes are listed in Supplementary Table S1.

2.12. ELISA for ANP

At the endpoint of ISO ± ANP treatment, plasma (collected into EDTA-coated tubes and centrifuged at 2,000 ×g, 10 min, 4 °C) were prepared. ANP concentrations were measured using a Mouse ANP ELISA kit (Arbor Assays, Ann Arbor, MI, USA) according to the manufacturer's instructions. Absorbance was read on a microplate reader (Infinite M200 microplate reader, Tecan Group Ltd., Männedorf, Switzerland), and concentrations were calculated from a standard curve (four-parameter logistic fit). Appropriate blanks and quality controls were included on each plate.

2.13. Data Presentation and Statistical Analysis

Data are shown as mean ± SEM; n denotes animals for in vivo studies and independent isolations for cell experiments. Two-group comparisons used unpaired two-tailed Student's t-tests, and multi-group comparisons used one- or two-way ANOVA with Tukey's post hoc tests as appropriate; correlations (e.g., plasma ANP vs HW/BW) used Pearson's r. A significance level of $p < 0.05$ was applied. Analyses were performed in GraphPad Prism 9 (GraphPad Software, San Diego, CA, USA) and OriginPro (OriginLab, Northampton, MA, USA).

3. Results

3.1. TRPM2 Is Enriched and Functionally Active in Atrial myocytes

RT–PCR detected Trpm2 transcripts in atria from wild-type (WT) hearts, whereas the band was absent in TRPM2$^{-/-}$ samples. In ventricular tissue, Trpm2 was not detectable under our RT–PCR conditions or, if present, near the threshold of detection (Figure 1A, Supplementary Figure 1). Consistently, in ventricular myocytes, ADPr failed to evoke a discernible current in either genotype (Supplementary Figure S1B–D).

In isolated atrial myocytes, intracellular ADPr (ADPr, 0.5 mM) elicited a time-dependent whole-cell current in WT cells, whereas currents remained minimal in WT cells dialyzed without ADPr and in TRPM2$^{-/-}$ cells irrespective of ADPr (Figure 1B). The ADPr-evoked current showed an approximately linear I–V relationship (Figure 1C). The increase in current density (ΔI) was significantly larger in WT + ADPr than in the other three conditions, which were near baseline (Figure 1D, $p < 0.05$). Consistently, exposure to H_2O_2 increased fura-2 ratios in WT atrial myocytes, whereas responses were markedly blunted in TRPM2$^{-/-}$ cells (Figures 1E, F, $p < 0.05$).

We did not detect ADPr/H_2O_2-activated currents in ventricular cardiomyocytes, consistent with our finding of barely detectable levels of TRPM2 channel expression in these cells.

3.2. TRPM2 Deficiency Aggravates ISO-Induced Systolic Dysfunction, Hypertrophy, and Fibrosis

Echocardiography revealed typical M-mode patterns across genotypes at baseline; during ISO administration, the contraction amplitude progressively decreased, most prominently in TRPM2$^{-/-}$ + ISO (Figure 2A). Fractional shortening (FS%) declined with ISO in both genotypes, but the reduction was significantly greater in TRPM2$^{-/-}$ mice (Figure 2B). Consistent indices are shown in Supplementary Figure S2: ejection fraction (EF) (Supplementary Figure S2A), heart rate (HR) (Supplementary Figure S2B), and left-ventricular end-systolic diameter (LVESD) (Supplementary Figure S2C), the latter increasing during ISO exposure. In contrast, left-ventricular end-diastolic diameter (LVEDD) showed no material change among groups (Figure 2C), indicating that the early impairment was largely systolic rather than dilatational.

 doi:10.20944/preprints202511.1147.v1

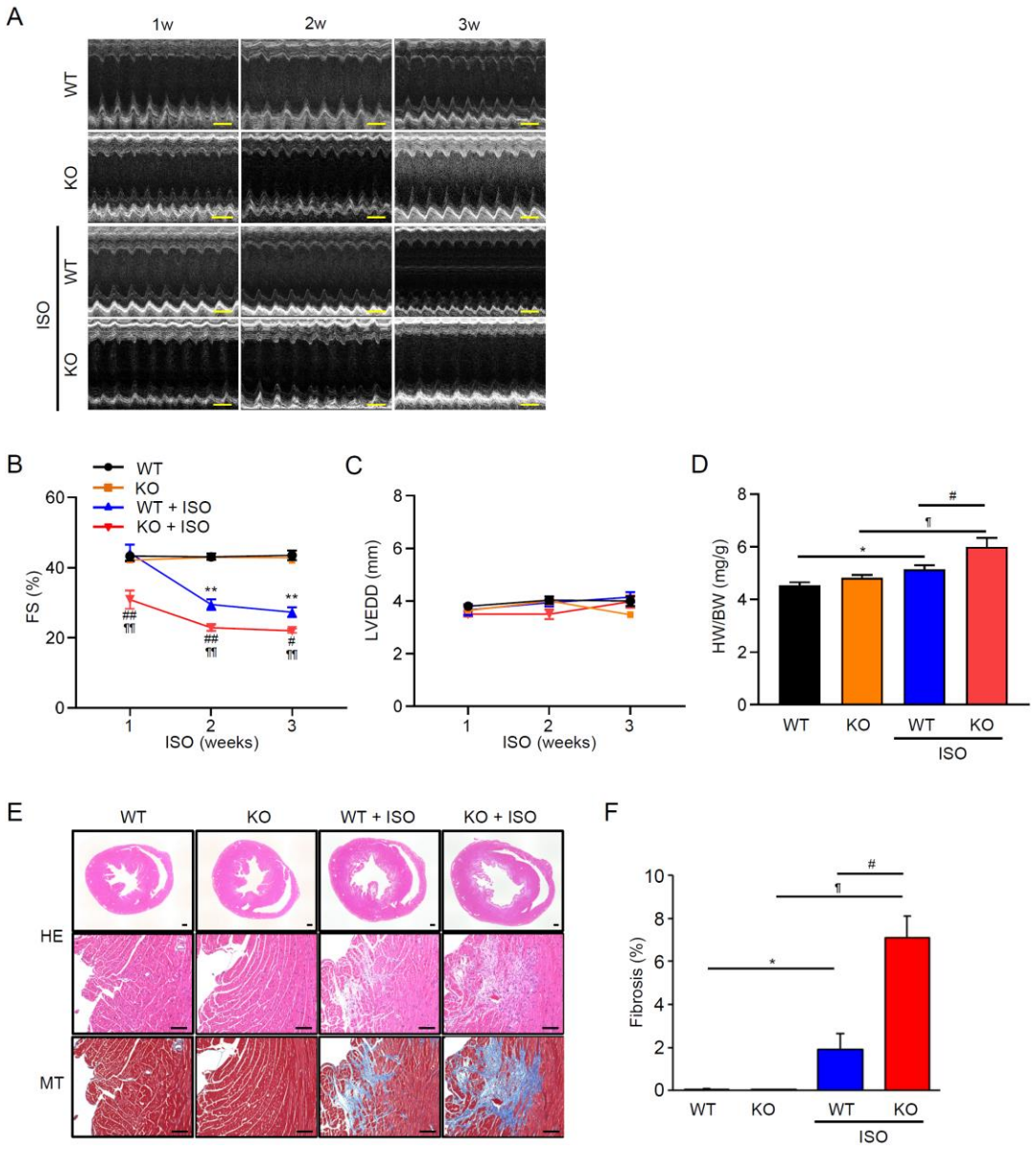

Figure 2. TRPM2 deficiency aggravates ISO-induced systolic dysfunction, hypertrophy, and fibrosis. (A) Representative M-mode echocardiograms (baseline, 1–3 weeks) in WT and TRPM2$^{-/-}$ (KO) mice. Scale bar (horizontal), 200 ms. (B) Time course of fractional shortening (FS, %). (C) Left-ventricular end-diastolic diameter (LVEDD, mm) over time. (D) Heart-weight–to–body-weight ratio (HW/BW) at endpoint. (E) Histology of whole-heart sections and mid-ventricular myocardium. Hematoxylin–eosin (HE) for myocyte morphology; Masson's trichrome (MT) for interstitial/perivascular collagen. Scale bars: 100 μm (upper panels), 500 μm (lower panels). (F) Quantification of fibrotic area (% of tissue). Dots represent individual animals. (B, D, F) $^{*}p < 0.05$, $^{**}p < 0.01$ WT vs WT + ISO; $^{¶}p < 0.05$, $^{¶¶}p < 0.01$ KO vs KO + ISO; $^{\#}p < 0.05$, $^{\#\#}p < 0.01$ WT + ISO vs KO + ISO.

Consistent with functional deterioration, heart weight/body weight (HW/BW) increased after ISO, with a larger gain in TRPM2$^{-/-}$ than in WT (Figure 2D). Histology supported these findings: hematoxylin–eosin (HE) sections showed myocardial enlargement after ISO in both genotypes, whereas Masson's trichrome (MT) staining demonstrated markedly greater interstitial fibrosis in TRPM2$^{-/-}$ + ISO (Figure 2E). Quantification confirmed a significant increase in fibrotic area only in TRPM2$^{-/-}$ mice, with a level higher than WT under ISO (Figure 2F).

Together, these results indicate that loss of TRPM2 exacerbates β-adrenergic stress–induced systolic dysfunction and pathological remodeling, with greater hypertrophy and fibrosis, while chamber size remains essentially unchanged over the observation period.

 doi:10.20944/preprints202511.1147.v1

3.3. β-Adrenergic Stress Evokes an ANP Program in WT Atria That Is Blunted in TRPM2$^{-/-}$

To probe upstream endocrine pathways, we performed bulk RNA-seq on atria from WT and TRPM2$^{-/-}$ mice with or without ISO. Standard analyses (quality control, alignment, differential expression) were followed by pathway enrichment/GSEA. In WT atria, ISO upregulated gene sets related to natriuretic peptide signaling and secretory granule/exocytosis, whereas these enrichments were attenuated in TRPM2$^{-/-}$ atria (Figure 3A, B, overview of typical analyses). As a focused visualization, Figure 3A is organized in two complementary heatmaps to identify TRPM2-dependent nodes within the ANP/secretory program. Left (ISO effect in WT): $\log_2$ fold-change for WT+ISO vs WT highlights genes induced by ISO in WT (red = up, blue = down). Right (ΔISO in KO–WT): the difference of ISO effects defined as ΔISO = (log2 (KO+ISO/KO)) − (log2(WT + ISO/WT)) so that negative values (blue) denote attenuation of the ISO response in KO relative to WT. By reading the two panels together, candidates for TRPM2-mediated regulation are genes that are red on the left (ISO-induced in WT) and blue on the right (ISO induction reduced in KO). Within the ANP-focused gene set (*Nppa*/*Nppb*, *Npr*1–3, *Corin*, *Furin*/*Pcsk* family, and vesicle-exocytosis components such as *Vamp*/*Snap*/*Syt*), this pattern includes *Nppa* (and to a lesser extent *Nppb*) together with selected processing/vesicle-fusion genes, consistent with a TRPM2-linked ANP granule/exocytosis module. Heatmaps display row-wise z-scores of $\log_2$[TPM+1] for visualization; statistical testing and orthogonal validation are provided by qPCR/ELISA in Figure 3B–D. For the matched 1-week cohort used for transcriptomics, representative histology and quantitative cardiac morphology are provided in Supplementary Figures 3A–C (HE/MT images, HW/BW, and fibrosis%).

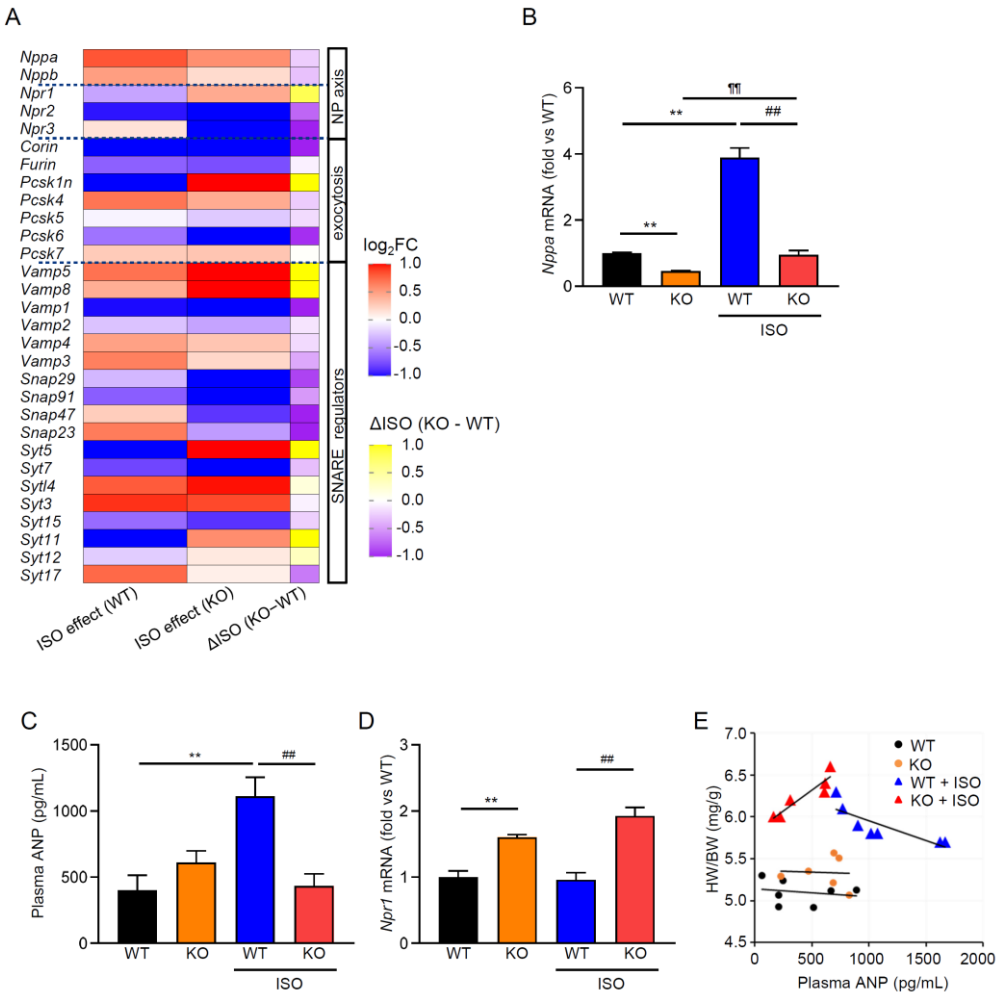

Figure 3. TRPM2 deficiency blunts the atrial ANP program under ISO. (A) Focused heatmap of ANP/secretory–exocytosis genes (*Nppa*, *Nppb*, *Npr1–3*, *Corin*, *Furin*/*Pcsk* family, *Vamp*/*Snap*/*Syt*) across WT, KO, WT+ISO,

 doi:10.20944/preprints202511.1147.v1

KO+ISO. Values are row-wise z-scores of $\log_2$(TPM+1); genes are clustered by Euclidean distance. ISO effect (WT) = $\log_2$FC (WT+ISO vs WT); ISO effect (KO) = $\log_2$FC (KO+ISO vs KO); ΔISO (KO−WT) = ISO effect (KO) − ISO effect (WT). (B) qPCR of *Nppa* (ANP) mRNA in atria (relative to WT). (C) Plasma ANP by ELISA. (D) Atrial *Npr1* (NPR-A) expression. (E) Correlation between plasma ANP and HW/BW. Linear least-squares fits of HW/BW (mg·g^{-1}) vs plasma ANP (pg·mL^{-1}): WT, $y = -1.0\times10^{-4}\,x + 5.14$; WT+ISO, $y = -5.0\times10^{-4}\,x + 6.43$; KO, $y = -4.0\times10^{-5}\,x + 5.36$; KO+ISO, $y = 1.0\times10^{-3}\,x + 5.83$. (B–D) $^{**}p < 0.01$ WT vs WT+ISO; ¶¶$p < 0.01$ KO vs KO+ISO; $^{\#\#}p < 0.01$ WT+ISO vs KO+ISO.

Consistent with the transcriptomic signal, qPCR confirmed that *Nppa* (ANP) expression rose markedly in WT + ISO, but the induction was significantly blunted in TRPM2$^{-/-}$ + ISO (Figure 3B). In plasma, ANP concentrations increased with ISO in WT and were lower in TRPM2$^{-/-}$ under the same stress (Figure 3C). By contrast, atrial Npr1 (NPR-A) expression showed no material reduction in TRPM2$^{-/-}$ (Figure 3D), indicating that the impaired endocrine response is not due to downregulation of the ANP receptor.

Across individual animals, plasma ANP showed an inverse relationship with HW/BW in WT during ISO exposure, whereas no clear inverse trend was observed in TRPM2$^{-/-}$ (Figure 3E). Together, these data indicate that, under β-adrenergic stress, TRPM2 contributes to the induction of the atrial ANP program and to the elevation of circulating ANP, and that loss of TRPM2 limits this cardioprotective endocrine response.

3.4. Exogenous ANP Mitigates ISO-Induced Dysfunction and Remodeling in TRPM2$^{-/-}$ Mice

To test whether the impaired endocrine (ANP) response contributes to the aggravated phenotype, we investigated how treatment with ANP (400 μg/kg/day, s.c., twice daily for 7 days) affects ISO-exposed TRPM2$^{-/-}$ mice. Mice treated with ANP showed improved systolic function compared with those that only received the vehicle control. FS% and EF% measures were also significantly higher in those that received ANP (Figure 4A–C). By contrast, chamber dimensions (LVEDD/LVESD) and heart rates were not affected by ANP treatment (Figure 4D–F). As for histological and morphometric measures, our data show that ANP modestly lowered HW/BW (Figure 4G) and attenuated histological remodeling in ISO-treated TRPM2$^{-/-}$ mice. Smaller myocyte profiles and less interstitial fibrosis are observed in HE and Masson's trichrome images, respectively (Figure 4H). Morphometric quantification confirmed that % fibrosis was indeed reduced in the presence of ANP (Figure 4I; $p < 0.05$). Overall, these results indicate that augmenting ANP signaling partially rescues ISO-induced systolic impairment and pathological remodeling in mice lacking TRPM2.

 doi:10.20944/preprints202511.1147.v1

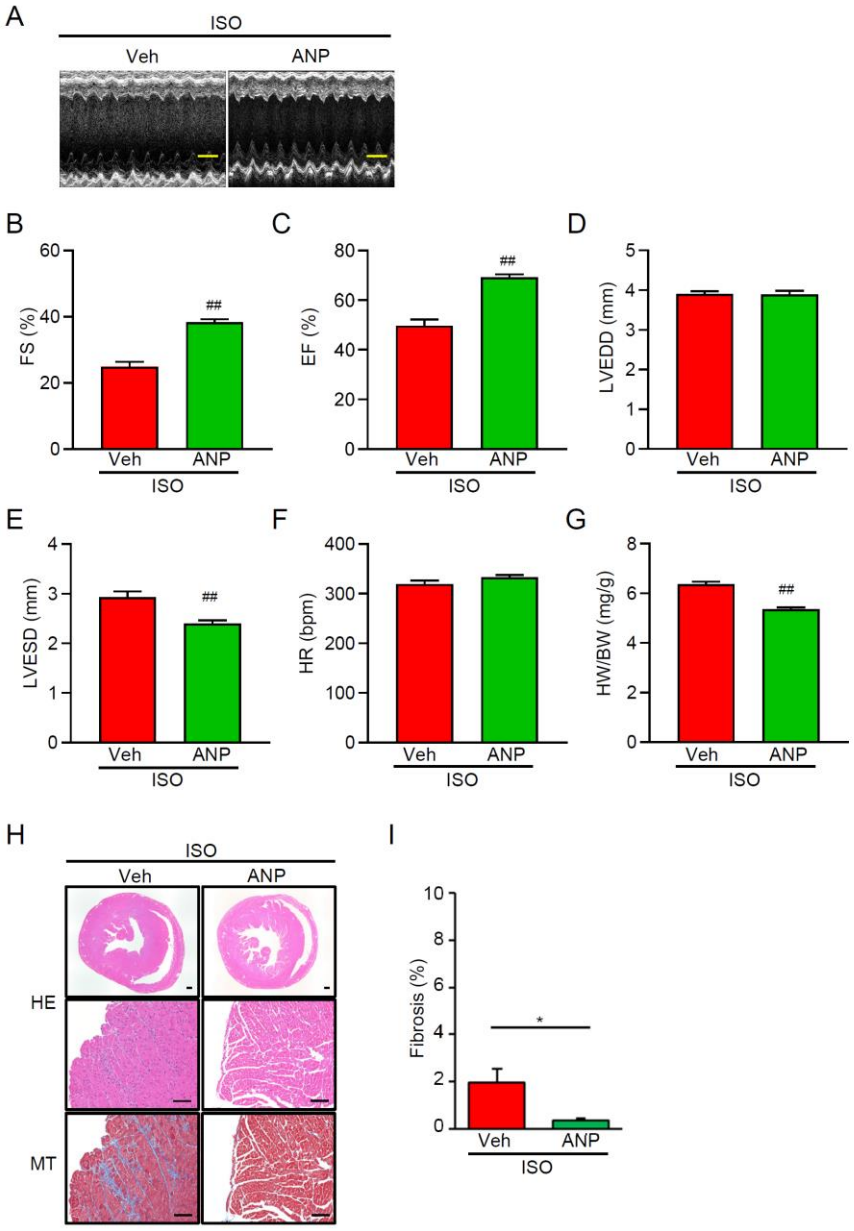

Figure 4. Exogenous ANP rescues dysfunction and remodeling in ISO-treated TRPM2$^{-/-}$ hearts. TRPM2$^{-/-}$ (KO) mice received ISO (30 mg·kg^{-1}·day^{-1}, i.p., 7 days) and were co-treated with vehicle or ANP (400 μg·kg^{-1}, s.c., 7 days). (A) Representative M-mode echocardiograms (Vehicle vs ANP). Scale bar (horizontal), 200 ms. (B–C) Fractional shortening (FS, %) and ejection fraction (EF, %) for Vehicle and ANP groups. (D–E) Left-ventricular diameters (LVEDD, LVESD, mm) for Vehicle and ANP groups. (F–G) Heart rate (HR, bpm) and heart-weight to body-weight ratio (HW/BW) for Vehicle and ANP groups. (H) Representative histology: H&E and Masson's trichrome (MT) sections. Scale bars: 100 μm (upper panels), 500 μm (lower panels). (I) Quantification of fibrosis area (% LV). (B-G, I) $^{*}p < 0.05$ Veh + ISO vs ANP + ISO; $^{\#\#}p < 0.01$ Veh + ISO vs ANP+ISO.

3.5. Ventricular Cardiomyocyte Hypertrophy Is Induced by ISO and Attenuated by ANP Irrespective of TRPM2

The finding that WT mice were able to mount a strong ANP response to ISO, whereas TRPM2$^{-/-}$ mice were unable to do so, suggests that TRPM2 plays a role in the induction of ANP. Given that atria are the major source of cardiac ANP, and the fact that we detected substantial TRPM2 expression only in atria, suggests that the effect of TRPM2 on ANP production may be limited to the atria. To test this hypothesis, we investigated the effects of ISO and ANP treatment on cultured neonatal ventricular myocytes from both WT and TRPM2$^{-/-}$ mice.

 doi:10.20944/preprints202511.1147.v1

Indeed, our results show comparable responsiveness of WT and TRPM2$^{-/-}$ to ISO and ANP exposure. As shown in Figures 5A, 5B, and 5D, ISO elicited a robust increase in cell cross-sectional area (CSA) in both WT and TRPM2$^{-/-}$ cells. Baseline CSA did not differ by genotype. Addition of ANP (0.1 μM) significantly but incompletely reduced ISO-induced hypertrophy in both genotypes (Figure 5C, D; $p < 0.05$ vs ISO), with CSA values typically remaining above control levels. There was no detectable genotype × treatment interaction for the ANP effect (WT vs KO, n.s.). Thus, ventricular ANP responsiveness appears preserved in the absence of TRPM2, consistent with the interpretation that the exacerbated in vivo remodeling in TRPM2$^{-/-}$ mice primarily reflects an atrial (endocrine) deficit in ANP induction rather than altered ventricular sensitivity to ANP.

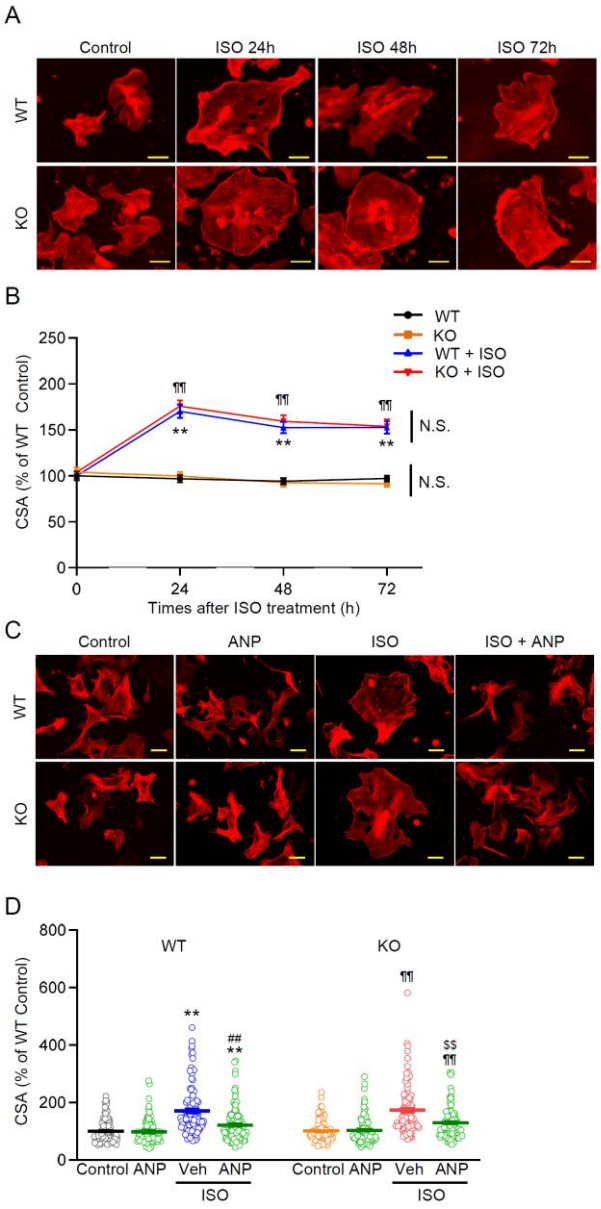

Figure 5. ISO-induced ventricular hypertrophy and its attenuation by ANP are comparable in WT and TRPM2$^{-/-}$ cardiomyocytes. (A) Representative images of neonatal ventricular myocytes (phalloidin, F-actin) from WT and TRPM2$^{-/-}$ (KO) mice under control conditions and after ISO (10 μM, 24–72 h). Scale bar, 50 μm. (B) Quantification of cell cross-sectional area (CSA) over 24–72 h, normalized to WT control; WT and TRPM2$^{-/-}$ were compared at each time point. (C) Representative images of cells with or without ANP (0.1 μM, 24 h) in basal and ISO-treated conditions. Scale bar, 50 μm. (D) CSA quantification across the indicated conditions for both genotypes. (B, D) $^{**}p < 0.01$ WT vs WT+ISO ± ANP; $^{¶¶}p < 0.01$ KO vs KO+ISO ± ANP; $^{\#\#}p < 0.01$ WT + ISO + Veh vs WT + ISO + ANP; $^{\$\$}p < 0.01$ KO + ISO + Veh vs KO + ISO + ANP; $^{N.S.}$ not significant.

 doi:10.20944/preprints202511.1147.v1

4. Discussion

This study reveals a previously unrecognized role of the TRPM2 channel in regulating cardiac endocrine function and protecting against stress-induced pathological remodeling. Known as a cellular sensor of oxidative stress and metabolic state, TRPM2 mediates the influx of Ca^{2+} and other cations in response to oxidative and metabolic stimuli (ADPr/H_2O_2; Figures 1B–F; see also TRPM2 activation by ADPr/oxidants in [14–17]). It is expressed in various cell types and tissues, including the heart, where it was shown to have both protective and detrimental effects [23,27]. The protective effect was attributed to TRPM2 serving as the influx pathway for Ca^{2+} required to maintain mitochondrial bioenergetics integrity after I/R injury [24,25].

Here, we show a novel cardioprotective mechanism for TRPM2, which is required for stress-evoked secretion of ANP, a key cardioprotective hormone. Loss of TRPM2 impairs ANP production under β-adrenergic stress, leading to exacerbated cardiac hypertrophy and fibrosis (Figure 2, Supplementary Figure S2). Importantly, we found that the addition of exogenous ANP restores the cardioprotective response in TRPM2$^{-/-}$ mice (Figure 4). This result strongly supports a crucial link between TRPM2 activity, stress-induced ANP secretion, and cardiac remodeling outcomes. Under our assay conditions, TRPM2 expression was predominantly detected in atria rather than in ventricles (Figure 1a, Supplementary Figure S1). It is noteworthy that ANP is also produced primarily in the atria by atrial cardiomyocytes in response to hemodynamic and mechanical stress. This increased ANP production is believed to be a protective hormonal response to maintain healthy myocardium and cardiovascular homeostasis. The ANP release is a regulated Ca^{2+}-dependent granule exocytotic process involving SNAREs on large dense-core vesicles [28,29]. Several ion channels and G-protein coupled receptors (GPCRs) are thought to regulate ANP secretion, although the influx pathway for the Ca^{2+} signal has not been identified.

Our studies comparing gene expression in WT and TRPM2$^{-/-}$ atria with or without ISO using bulk RNA-seq revealed activation of secretory/exocytotic pathways in WT + ISO, with attenuated induction in TRPM2$^{-/-}$ + ISO, and a blunted upregulation of the ANP program (e.g., *Nppa*) in the absence of TRPM2 (Figures 3A, B). The ANP receptor gene, Npr1 (NPR-A), did not appear to be affected by the absence of TRPM2. Its expression was maintained or just modestly increased under ISO in TRPM2$^{-/-}$ atria. These results potentially reflect a compensatory/negative-feedback response to reduced ANP availability, and are consistent with our qPCR data (Figure 3D). These gene expression studies, combined with electrophysiology and Ca^{2+} imaging data on WT and TRPM2$^{-/-}$ atrial cardiomyocytes, collectively identify TRPM2 as an upstream component linking β-adrenergic stress to endocrine (ANP) output. In heart atria, TRPM2 has a specialized endocrine role distinct from that of more broadly expressed cardiac ion channels. Our data support a model in which TRPM2 supplies the stress-evoked Ca^{2+} input upstream of regulated ANP exocytosis. This interpretation is compatible with recent evidence that the regulated exocytic machinery controls ANP release in cardiomyocytes [30,31] and with reports that NPR-A expression is downregulated by ligand/cGMP [32], providing a rationale for higher Npr1 when ANP is limited in TRPM2 deficiency.

Beyond the atrial context, there is precedent for TRPM2 coupling metabolic/oxidative cues to secretory output in endocrine and immune cells. In pancreatic β-cells, TRPM2 is co-expressed with insulin, and its activity is potentiated by physiological warmth and cyclic ADPr; mild heating elevates cytosolic Ca^{2+} and promotes insulin release, an effect diminished by TRPM2 knockdown [33]. In macrophages, TRPM2 forms part of a redox–ADPr negative-feedback loop that restrains cytokine production and secretion upon inflammatory polarization, with TRPM2 deficiency augmenting the output of IL-1α/IL-6/TNF-α output [34]. Together, these reports support a generalizable role for TRPM2 as a stress-responsive gate that links ADPr/redox signals to regulated secretion, lending independent plausibility to our conclusion that TRPM2 operates upstream of stress-evoked ANP release in atrial cardiomyocytes.

In clinical practice, short-term infusion of recombinant human ANP (carperitide) is used for acute decompensated heart failure and produces prompt hemodynamic unloading—reductions in pulmonary capillary wedge pressure and systemic vascular resistance with increased stroke volume

 doi:10.20944/preprints202511.1147.v1

index—together with natriuresis/diuresis and an acceptable safety profile (82% clinical improvement in a 3,777-patient registry; hypotension the main adverse event) [35–37]. While the short-term hemodynamic and decongestive effects are consistent, the longer-term clinical benefit remains uncertain. Extensive observational analyses and a recent meta-analysis show no apparent mortality reduction and, in some cohorts, higher in-hospital mortality [38–40]. In our study, exogenous ANP rescued ISO-induced dysfunction, hypertrophy, and fibrosis in TRPM2$^{-/-}$ mice (Figure 4), supporting the idea that when endogenous ANP release is insufficient—such as during acute sympathetic/oxidative stress—ANP supplementation can restore a cardioprotective endocrine response. These findings raise the possibility that patients with impaired atrial TRPM2–ANP signaling might particularly benefit from early augmentation of the ANP axis (e.g., ANP administration, neprilysin inhibition, or future TRPM2-enhancing strategies), a hypothesis that warrants prospective testing.

Given the established view of the heart as an endocrine organ governed by the natriuretic peptide system [12,41,42], our findings extend TRPM2 beyond its classical roles in oxidative-stress sensing and I/R paradigms [19,24,25,43–45] by highlighting an atrial endocrine function. From a translational standpoint, approaches that enhance TRPM2-dependent signaling in atrial cells or otherwise amplify the ANP axis could help boost ANP output and mitigate pathological remodeling in heart failure or hypertension.

This work focuses on atrial cardiomyocytes, positioning TRPM2 as part of the ANP granule/regulated exocytosis mechanism. While functional activation (Figure 1) is consistent with plasma-membrane localization, we did not demonstrate co-localization with ANP granules or molecular coupling to the exocytic machinery. The in vivo gating dynamics of atrial TRPM2 under ISO—including possible ROS/ADPr microdomains—remain undefined, and it is unknown whether these atrial findings generalize to pressure overload or myocardial infarction. Notably, in neonatal ventricular myocytes, exogenous ANP attenuated ISO-induced hypertrophy independently of TRPM2 (Figure 5A–D), suggesting that TRPM2 is not required for downstream ANP actions in ventricles, but is essential upstream for stress-evoked ANP production in atria.

5. Conclusions

Together, these findings support a TRPM2–Ca^{2+}–ANP axis in which atrial TRPM2 supplies the stress-evoked Ca^{2+} input that facilitates endocrine ANP output—rather than modulating ANP responsiveness per se. To our knowledge, this is the first report of TRPM2 as a regulator of atrial endocrine signaling and a gatekeeper of cardioprotective ANP release under β-adrenergic stress, suggesting a tractable therapeutic target for stress-induced cardiac dysfunction.

Supplementary Materials: The following supporting information can be downloaded at the website of this paper posted on Preprints.org, Figure S1: RT-PCR of cardiac chambers; Figure S2: Additional echocardiographic indices corresponding to Figure 2; Figure S3: Additional histology and quantification corresponding to Figure 3; Table S1: t Primer sets used for RT-PCR/qPCR.

Author Contributions: TN: Conceptualization, Supervision, Project administration, Methodology, Formal Analysis, Funding acquisition, Investigation, Visualization, Writing—original draft, Writing—review and editing. HT: Funding acquisition, Investigation, Methodology, Formal Analysis, Visualization, Writing—review and editing. KS-N: Data curation, Validation, Writing—review and editing. MCH: Resources, Conceptual advice on TRPM2 biology, Writing—review and editing. FA: Investigation; Data curation; Visualization; Writing—review & editing. AS: Investigation; Formal analysis; Resources; Writing—review & editing. SY: Resources; Methodological support; Writing—review & editing. HW: Histological analysis, Experimental support, Writing—review & editing.

Funding: This work was supported by JSPS KAKENHI (Grant Numbers 23136505 and 25136708, to T.N. and 22K06659, 22K06659DK to H.T.) and by JKA through its promotion funds for KEIRIN RACE (to T.N.). The funders had no role in study design, data collection and analysis, decision to publish, or manuscript preparation.

 doi:10.20944/preprints202511.1147.v1

Institutional Review Board Statement: All animal experiments were conducted in accordance with institutional guidelines and approved by the Animal Ethics Committee of Akita University (Akita, Japan; approval numbers: a-1-0412 and b-1-0408).

Informed Consent Statement: Not applicable.

Data Availability Statement: The RNA-seq datasets generated in this study have been submitted to the NCBI Sequence Read Archive (SRA) under submission ID SUB15770329 and will be made publicly available upon acceptance. Final accession numbers will be provided in the published article. Source data underlying all figures and analysis scripts are available from the corresponding author upon reasonable request.

Acknowledgments: The authors thank Satomi Akabane and Takao Shioya for instructing us in cardiac tissue isolation. We also thank Rina Tanaka for her early assistance with patch-clamp setup and recordings.

Conflicts of Interest: The authors declare that the research was conducted in the absence of any commercial or financial relationships that could be construed as a potential conflict of interest.

Abbreviations

The following abbreviations are used in this manuscript:

ADPr	ADP-ribose
ANOVA	Analysis of variance
ANP	Atrial natriuretic peptide
BSA	Bovine serum albumin
cADPr	Cyclic ADP-ribose
CSA	Cross-sectional area
DMEM	Dulbecco's Modified Eagle Medium
EF	Ejection fraction
ELISA	Enzyme-linked immunosorbent assay
FS	Fractional shortening
GEO	Gene Expression Omnibus
GO	Gene Ontology
GPCR	G-protein-coupled receptor
GSEA	Gene Set Enrichment Analysis
H&E	Hematoxylin and eosin
HEPES	4-(2-Hydroxyethyl)-1-piperazineethanesulfonic acid
HR	Heart rate
HW/BW	Heart weight-to-body weight ratio
H_2O_2	Hydrogen peroxide
I/R	Ischemia–reperfusion
I–V	Current–voltage
ISO	Isoproterenol
KEGG	Kyoto Encyclopedia of Genes and Genomes
KO	Knockout
LVEDD	Left-ventricular end-diastolic diameter
LVESD	Left-ventricular end-systolic diameter
MT	Masson's trichrome
NES	Normalized enrichment score
NMVMs	Neonatal mouse ventricular myocytes
NPR-A/-B/-C	Natriuretic peptide receptor A/B/C (Npr1/Npr2/Npr3)
Nppa/Nppb	Genes encoding ANP/BNP precursors
NUDT9-H	NUDT9-homology domain
PARP/PARG	Poly(ADP-ribose) polymerase / glycohydrolase
PBS	Phosphate-buffered saline
Pyk2	Proline-rich tyrosine kinase 2
qPCR	Quantitative polymerase chain reaction
RNA-seq	RNA sequencing
ROS	Reactive oxygen species

 doi:10.20944/preprints202511.1147.v1

RT-PCR	Reverse-transcription polymerase chain reaction
SEM	Standard error of the mean
SNARE	Soluble NSF Attachment Protein Receptor
SRA	Sequence Read Archive
SYT	Synaptotagmin
TPM	Transcripts per million
TRPM2	Transient receptor potential melastatin-2
VAMP	Vesicle-associated membrane protein
Veh	Vehicle
WT	Wild type
bpm	Beats per minute
bp	Base pairs
i.p.	Intraperitoneal
s.c.	Subcutaneous
N.S.	Not significant

References

3. de Lucia, C.; Eguchi, A.; Koch, W.J. New Insights in Cardiac β-Adrenergic Signaling During Heart Failure and Aging. Front Pharmacol 2018, 9, 904, doi:10.3389/fphar.2018.00904.
4. Rosenkranz, S.; Flesch, M.; Amann, K.; Haeuseler, C.; Kilter, H.; Seeland, U.; Schlüter, K.D.; Böhm, M. Alterations of beta-adrenergic signaling and cardiac hypertrophy in transgenic mice overexpressing TGF-beta(1). Am J Physiol Heart Circ Physiol 2002, 283, H1253-1262, doi:10.1152/ajpheart.00578.2001.
5. Caturano, A.; Vetrano, E.; Galiero, R.; Salvatore, T.; Docimo, G.; Epifani, R.; Alfano, M.; Sardu, C.; Marfella, R.; Rinaldi, L.; et al. Cardiac Hypertrophy: From Pathophysiological Mechanisms to Heart Failure Development. Rev Cardiovasc Med 2022, 23, 165, doi:10.31083/j.rcm2305165.
6. He, X.; Du, T.; Long, T.; Liao, X.; Dong, Y.; Huang, Z.P. Signaling cascades in the failing heart and emerging therapeutic strategies. Signal Transduct Target Ther 2022, 7, 134, doi:10.1038/s41392-022-00972-6.
7. Kehat, I.; Molkentin, J.D. Molecular Pathways Underlying Cardiac Remodeling During Pathophysiological Stimulation. Circulation 2010, 122, 2727-2735, doi:10.1161/CIRCULATIONAHA.110.942268.
8. Takimoto, E.; Kass, D.A. Role of Oxidative Stress in Cardiac Hypertrophy and Remodeling. Hypertension 2007, 49, 241-248, doi:10.1161/01.HYP.0000254415.31362.a7.
9. Brown, D.I.; Griendling, K.K. Regulation of signal transduction by reactive oxygen species in the cardiovascular system. Circ Res 2015, 116, 531-549, doi:10.1161/circresaha.116.303584.
10. Burgoyne, J.R.; Mongue-Din, H.; Eaton, P.; Shah, A.M. Redox signaling in cardiac physiology and pathology. Circ Res 2012, 111, 1091-1106, doi:10.1161/circresaha.111.255216.
11. Dai, D.F.; Chen, T.; Johnson, S.C.; Szeto, H.; Rabinovitch, P.S. Cardiac aging: from molecular mechanisms to significance in human health and disease. Antioxid Redox Signal 2012, 16, 1492-1526, doi:10.1089/ars.2011.4179.
12. Tsutsui, H.; Kinugawa, S.; Matsushima, S. Oxidative stress and heart failure. Am J Physiol Heart Circ Physiol 2011, 301, H2181-2190, doi:10.1152/ajpheart.00554.2011.
13. Forte, M.; Madonna, M.; Schiavon, S.; Valenti, V.; Versaci, F.; Zoccai, G.B.; Frati, G.; Sciarretta, S. Cardiovascular Pleiotropic Effects of Natriuretic Peptides. Int J Mol Sci 2019, 20, doi:10.3390/ijms20163874.
14. Goetze, J.P.; Bruneau, B.G.; Ramos, H.R.; Ogawa, T.; de Bold, M.K.; de Bold, A.J. Cardiac natriuretic peptides. Nat Rev Cardiol 2020, 17, 698-717, doi:10.1038/s41569-020-0381-0.
15. Sarzani, R.; Allevi, M.; Di Pentima, C.; Schiavi, P.; Spannella, F.; Giulietti, F. Role of Cardiac Natriuretic Peptides in Heart Structure and Function. Int J Mol Sci 2022, 23, doi:10.3390/ijms232214415.
16. Fonfria, E.; Marshall, I.C.; Benham, C.D.; Boyfield, I.; Brown, J.D.; Hill, K.; Hughes, J.P.; Skaper, S.D.; McNulty, S. TRPM2 channel opening in response to oxidative stress is dependent on activation of poly(ADP-ribose) polymerase. Br J Pharmacol 2004, 143, 186-192, doi:10.1038/sj.bjp.0705914.
17. Perraud, A.L.; Takanishi, C.L.; Shen, B.; Kang, S.; Smith, M.K.; Schmitz, C.; Knowles, H.M.; Ferraris, D.; Li, W.; Zhang, J.; et al. Accumulation of free ADP-ribose from mitochondria mediates oxidative stress-induced gating of TRPM2 cation channels. J Biol Chem 2005, 280, 6138-6148, doi:10.1074/jbc.M411446200.

 doi:10.20944/preprints202511.1147.v1

18. Hecquet, C.M.; Malik, A.B. Role of H(2)O(2)-activated TRPM2 calcium channel in oxidant-induced endothelial injury. Thromb Haemost 2009, 101, 619-625.
19. Numata, T.; Sato, K.; Christmann, J.; Marx, R.; Mori, Y.; Okada, Y.; Wehner, F. The ΔC splice-variant of TRPM2 is the hypertonicity-induced cation channel in HeLa cells, and the ecto-enzyme CD38 mediates its activation. J Physiol 2012, 590, 1121-1138, doi:10.1113/jphysiol.2011.220947.
20. Miller, B.A.; Wang, J.; Hirschler-Laszkiewicz, I.; Gao, E.; Song, J.; Zhang, X.Q.; Koch, W.J.; Madesh, M.; Mallilankaraman, K.; Gu, T.; et al. The second member of transient receptor potential-melastatin channel family protects hearts from ischemia-reperfusion injury. Am J Physiol Heart Circ Physiol 2013, 304, H1010-1022, doi:10.1152/ajpheart.00906.2012.
21. Huang, P.; Qu, C.; Rao, Z.; Wu, D.; Zhao, J. Bidirectional regulation mechanism of TRPM2 channel: role in oxidative stress, inflammation and ischemia-reperfusion injury. Front Immunol 2024, 15, 1391355, doi:10.3389/fimmu.2024.1391355.
22. Zielińska, W.; Zabrzyński, J.; Gagat, M.; Grzanka, A. The Role of TRPM2 in Endothelial Function and Dysfunction. Int J Mol Sci 2021, 22, doi:10.3390/ijms22147635.
23. Hara, Y.; Wakamori, M.; Ishii, M.; Maeno, E.; Nishida, M.; Yoshida, T.; Yamada, H.; Shimizu, S.; Mori, E.; Kudoh, J.; et al. LTRPC2 Ca^{2+}-permeable channel activated by changes in redox status confers susceptibility to cell death. Mol Cell 2002, 9, 163-173, doi:10.1016/s1097-2765(01)00438-5.
24. Perraud, A.L.; Fleig, A.; Dunn, C.A.; Bagley, L.A.; Launay, P.; Schmitz, C.; Stokes, A.J.; Zhu, Q.; Bessman, M.J.; Penner, R.; et al. ADP-ribose gating of the calcium-permeable LTRPC2 channel revealed by Nudix motif homology. Nature 2001, 411, 595-599, doi:10.1038/35079100.
25. Hoffman, N.E.; Miller, B.A.; Wang, J.; Elrod, J.W.; Rajan, S.; Gao, E.; Song, J.; Zhang, X.Q.; Hirschler-Laszkiewicz, I.; Shanmughapriya, S.; et al. Ca^{2+} entry via Trpm2 is essential for cardiac myocyte bioenergetics maintenance. Am J Physiol Heart Circ Physiol 2015, 308, H637-650, doi:10.1152/ajpheart.00720.2014.
26. Miller, B.A.; Hoffman, N.E.; Merali, S.; Zhang, X.Q.; Wang, J.; Rajan, S.; Shanmughapriya, S.; Gao, E.; Barrero, C.A.; Mallilankaraman, K.; et al. TRPM2 channels protect against cardiac ischemia-reperfusion injury: role of mitochondria. J Biol Chem 2014, 289, 7615-7629, doi:10.1074/jbc.M113.533851.
27. Miller, B.A.; Wang, J.; Song, J.; Zhang, X.Q.; Hirschler-Laszkiewicz, I.; Shanmughapriya, S.; Tomar, D.; Rajan, S.; Feldman, A.M.; Madesh, M.; et al. Trpm2 enhances physiological bioenergetics and protects against pathological oxidative cardiac injury: Role of Pyk2 phosphorylation. J Cell Physiol 2019, 234, 15048-15060, doi:10.1002/jcp.28146.
28. Guo, X.; Wang, P.; Wei, H.; Yan, J.; Zhang, D.; Qian, Y.; Guo, B. Interleukin(IL)-37 attenuates isoproterenol (ISO)-induced cardiac hypertrophy by suppressing JAK2/STAT3-signaling associated inflammation and oxidative stress. Int Immunopharmacol 2024, 142, 113134, doi:10.1016/j.intimp.2024.113134.
29. Hiroi, T.; Wajima, T.; Negoro, T.; Ishii, M.; Nakano, Y.; Kiuchi, Y.; Mori, Y.; Shimizu, S. Neutrophil TRPM2 channels are implicated in the exacerbation of myocardial ischaemia/reperfusion injury. Cardiovascular Research 2012, 97, 271-281, doi:10.1093/cvr/cvs332.
30. Ferlito, M.; Fulton, W.B.; Zauher, M.A.; Marbán, E.; Steenbergen, C.; Lowenstein, C.J. VAMP-1, VAMP-2, and syntaxin-4 regulate ANP release from cardiac myocytes. Journal of Molecular and Cellular Cardiology 2010, 49, 791-800, doi:https://doi.org/10.1016/j.yjmcc.2010.08.020.
31. Peters, C.G.; Miller, D.F.; Giovannucci, D.R. Identification, localization and interaction of SNARE proteins in atrial cardiac myocytes. Journal of Molecular and Cellular Cardiology 2006, 40, 361-374, doi:https://doi.org/10.1016/j.yjmcc.2005.12.007.
32. Essandoh, K.; Eramo, G.A.; Subramani, A.; Brody, M.J. Rab3gap1 palmitoylation cycling modulates cardiomyocyte exocytosis and atrial natriuretic peptide release. Biophys J 2025, 124, 1843-1855, doi:10.1016/j.bpj.2025.02.010.
33. Essandoh, K.; Subramani, A.; Koripella, S.; Brody, M.J. The Rab3 GTPase cycle modulates cardiomyocyte exocytosis and atrial natriuretic peptide release. Biophys J 2025, 124, 1856-1866, doi:10.1016/j.bpj.2025.03.013.

 doi:10.20944/preprints202511.1147.v1

34. Cao, L.; Chen, S.C.; Cheng, T.; Humphreys, M.H.; Gardner, D.G. Ligand-dependent regulation of NPR-A gene expression in inner medullary collecting duct cells. American Journal of Physiology-Renal Physiology 1998, 275, F119-F125, doi:10.1152/ajprenal.1998.275.1.F119.
35. Togashi, K.; Hara, Y.; Tominaga, T.; Higashi, T.; Konishi, Y.; Mori, Y.; Tominaga, M. TRPM2 activation by cyclic ADP-ribose at body temperature is involved in insulin secretion. Embo j 2006, 25, 1804-1815, doi:10.1038/sj.emboj.7601083.
36. Rajan, S.; Shalygin, A.; Gudermann, T.; Chubanov, V.; Dietrich, A. TRPM2 channels are essential for regulation of cytokine production in lung interstitial macrophages. Journal of Cellular Physiology 2024, 239, e31322, doi:https://doi.org/10.1002/jcp.31322.
37. Saito, Y.; Nakao, K.; Nishimura, K.; Sugawara, A.; Okumura, K.; Obata, K.; Sonoda, R.; Ban, T.; Yasue, H.; Imura, H. Clinical application of atrial natriuretic polypeptide in patients with congestive heart failure: beneficial effects on left ventricular function. Circulation 1987, 76, 115-124, doi:10.1161/01.cir.76.1.115.
38. Suwa, M.; Seino, Y.; Nomachi, Y.; Matsuki, S.; Funahashi, K. Multicenter prospective investigation on efficacy and safety of carperitide for acute heart failure in the 'real world' of therapy. Circ J 2005, 69, 283-290, doi:10.1253/circj.69.283.
39. Wang, G.; Wang, P.; Li, Y.; Liu, W.; Bai, S.; Zhen, Y.; Li, D.; Yang, P.; Chen, Y.; Hong, L.; et al. Efficacy and Safety of 1-Hour Infusion of Recombinant Human Atrial Natriuretic Peptide in Patients With Acute Decompensated Heart Failure: A Phase III, Randomized, Double-Blind, Placebo-Controlled, Multicenter Trial. Medicine (Baltimore) 2016, 95, e2947, doi:10.1097/md.0000000000002947.
40. Khan, A.; Rath, S.; Waqas, S.A.; Alam, U.; Ali, M.A.; Khadim, S.; Akbar, U.A.; Laghari, M.A.; Collins, P.; Ahmed, R. Effect of carperitide on mortality and ANP levels in acute heart failure: A systematic review and meta-analysis. American Heart Journal Plus: Cardiology Research and Practice 2025, 59, 100624, doi:https://doi.org/10.1016/j.ahjo.2025.100624.
41. Matsue, Y.; Kagiyama, N.; Yoshida, K.; Kume, T.; Okura, H.; Suzuki, M.; Matsumura, A.; Yoshida, K.; Hashimoto, Y. Carperitide Is Associated With Increased In-Hospital Mortality in Acute Heart Failure: A Propensity Score-Matched Analysis. J Card Fail 2015, 21, 859-864, doi:10.1016/j.cardfail.2015.05.007.
42. Nagai, T.; Iwakami, N.; Nakai, M.; Nishimura, K.; Sumita, Y.; Mizuno, A.; Tsutsui, H.; Ogawa, H.; Anzai, T. Effect of intravenous carperitide versus nitrates as first-line vasodilators on in-hospital outcomes in hospitalized patients with acute heart failure: Insight from a nationwide claim-based database. Int J Cardiol 2019, 280, 104-109, doi:10.1016/j.ijcard.2019.01.049.
43. Clerico, A.; Giannoni, A.; Vittorini, S.; Passino, C. Thirty years of the heart as an endocrine organ: physiological role and clinical utility of cardiac natriuretic hormones. Am J Physiol Heart Circ Physiol 2011, 301, H12-20, doi:10.1152/ajpheart.00226.2011.
44. Volpe, M.; Gallo, G.; Rubattu, S. Endocrine functions of the heart: from bench to bedside. Eur Heart J 2023, 44, 643-655, doi:10.1093/eurheartj/ehac759.
45. Malko, P.; Jiang, L.H. TRPM2 channel-mediated cell death: An important mechanism linking oxidative stress-inducing pathological factors to associated pathological conditions. Redox Biol 2020, 37, 101755, doi:10.1016/j.redox.2020.101755.
46. Zhan, K.Y.; Yu, P.L.; Liu, C.H.; Luo, J.H.; Yang, W. Detrimental or beneficial: the role of TRPM2 in ischemia/reperfusion injury. Acta Pharmacol Sin 2016, 37, 4-12, doi:10.1038/aps.2015.141.
47. Zhong, C.; Yang, J.; Zhang, Y.; Fan, X.; Fan, Y.; Hua, N.; Li, D.; Jin, S.; Li, Y.; Chen, P.; et al. TRPM2 Mediates Hepatic Ischemia-Reperfusion Injury via $Ca^{(2+)}$-Induced Mitochondrial Lipid Peroxidation through Increasing ALOX12 Expression. Research (Wash D C) 2023, 6, 0159, doi:10.34133/research.0159.